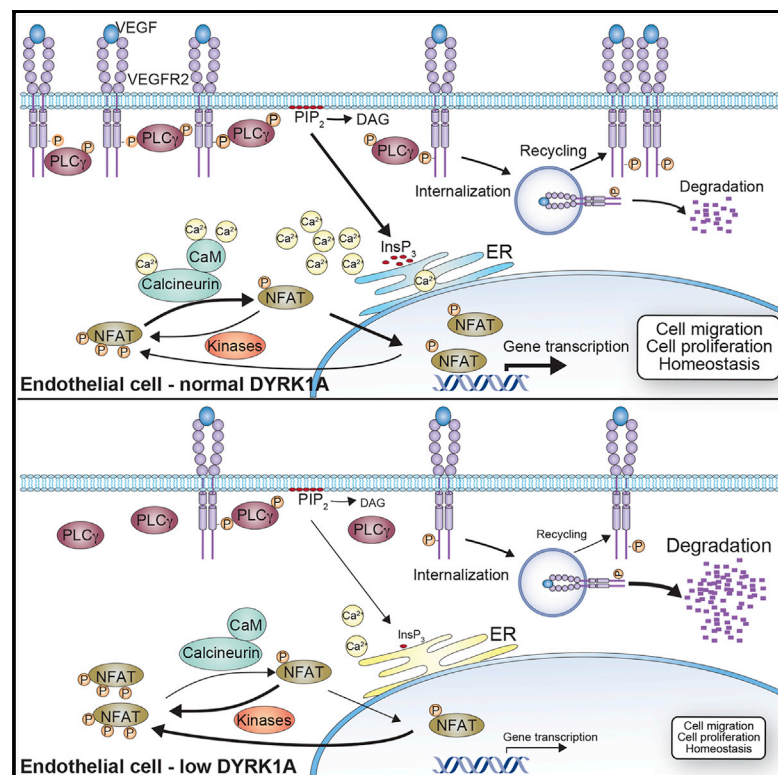# Cell Reports

DYRK1A Kinase Positively Regulates Angiogenic Responses in Endothelial Cells

Graphical Abstract

Authors

Esteban J. Rozen, Julia Roewenstrunk, María José Barallobre, ..., Mariona Graupera, Miguel A. Valverde, Susana de la Luna

Correspondence

susana.luna@crg.eu

In Brief

Dysregulation of DYRK1A kinase expression leads to disease in humans; its overexpression is linked to Down syndrome pathological traits, and its haploinsufficiency causes a clinical syndrome. Rozen et al. show that normal levels of DYRK1A are required for physiological angiogenesis, acting positively on VEGF-dependent NFAT transcription in endothelial cells.

Highlights

- DYRK1A positively regulates VEGF-dependent NFAT transcription in endothelial cells

- DYRK1A silencing reduces intracellular Ca^{2+} influx in response to VEGF

- VEGFR2 accumulation is reduced when DYRK1A is downregulated

- *Dyrk1a* heterozygous mice show defects in developmental retinal vascularization

CellPress

Article

DYRK1A Kinase Positively Regulates Angiogenic Responses in Endothelial Cells

Esteban J. Rozen,[1,2,10] Julia Roewenstrunk,[1,2,10] María José Barallobre,[2,3,10] Chiara Di Vona,[1,2,10] Carole Jung,[4] Ana F. Figueiredo,[5] Jeroni Luna,[2,6] Cristina Fillat,[2,6,7] Maria L. Arbonés,[2,3] Mariona Graupera,[5,8] Miguel A. Valverde,[4] and Susana de la Luna[1,2,9,11,*]

[1]Centre for Genomic Regulation (CRG), The Barcelona Institute of Science and Technology, 08003 Barcelona, Spain
[2]Centro de Investigación Biomédica en Red en Enfermedades Raras (CIBERER), Spain
[3]Institut de Biologia Molecular de Barcelona (IBMB), 08028 Barcelona, Spain
[4]Laboratory of Molecular Physiology, Department of Experimental and Health Sciences, Universitat Pompeu Fabra (UPF), 08003 Barcelona, Spain
[5]Vascular Signaling Laboratory, ProCURE and Oncobell Programs, Institut d'Investigació Biomèdica de Bellvitge (IDIBELL), 08907 L'Hospitalet de Llobregat, Barcelona, Spain
[6]Institut D'Investigacions Biomèdiques August Pi i Sunyer (IDIBAPS), 08036 Barcelona, Spain
[7]Facultat de Medicina i Ciències de la Salut. Universitat de Barcelona (UB), 08036 Barcelona, Spain
[8]Centro de Investigación Biomédica en Red en Cáncer (CIBERONC), Spain
[9]Institució Catalana de Recerca i Estudis Avançats (ICREA), 08010 Barcelona, Spain
[10]These authors contributed equally
[11]Lead Contact
*Correspondence: susana.luna@crg.eu
https://doi.org/10.1016/j.celrep.2018.04.008

SUMMARY

Angiogenesis is a highly regulated process essential for organ development and maintenance, and its deregulation contributes to inflammation, cardiac disorders, and cancer. The Ca^{2+}/nuclear factor of activated T cells (NFAT) signaling pathway is central to endothelial cell angiogenic responses, and it is activated by stimuli like vascular endothelial growth factor (VEGF) A. NFAT phosphorylation by dual-specificity tyrosine phosphorylation-regulated kinases (DYRKs) is thought to be an inactivating event. Contrary to expectations, we show that the DYRK family member DYRK1A positively regulates VEGF-dependent NFAT transcriptional responses in primary endothelial cells. DYRK1A silencing reduces intracellular Ca^{2+} influx in response to VEGF, which dampens NFAT activation. The effect is exerted at the level of VEGFR2 accumulation leading to impairment in PLCγ1 activation. Notably, *Dyrk1a* heterozygous mice show defects in developmental retinal vascularization. Our data establish a regulatory circuit, DYRK1A/ Ca^{2+}/NFAT, to fine-tune endothelial cell proliferation and angiogenesis.

INTRODUCTION

Vascular endothelial growth factor (VEGF) is the principal regulator of new blood vessel sprouting, promoting a range of cellular responses in endothelial cells (ECs) that include survival, proliferation, migration, invasion, and/or permeability (reviewed in Herbert and Stainier, 2011). VEGF exerts its effects by activating its cognate tyrosine kinase receptor, VEGFR (encoded by the *KDR*,

FLT1, and *FLT4* genes), which thereafter engages multiple intracellular signaling cascades that include the extracellular regulated kinase/mitogen-activated protein kinases (ERK/MAPKs), the phosphoinositide 3-kinase (PI3K)/AKT pathway, or the phospholipase Cγ (PLCγ)/Ca^{2+} pathway (reviewed in Simons et al., 2016). The PLCγ/Ca^{2+} pathway is responsible for the opening of the Ca^{2+} channel receptors in the endoplasmic reticulum (ER) membrane and the subsequent opening of Ca^{2+} channels in the plasma membrane that leads to an increase in intracellular Ca^{2+} (reviewed in Soboloff et al., 2012). This event activates the phosphatase calcineurin (CN), which leads to the dephosphorylation of the nuclear factor of activated T cells (NFAT) family of transcription factors and its relocalization to the nucleus, where it regulates the transcription of target genes central to angiogenesis (reviewed in Müller and Rao, 2010). A number of kinases are known to modulate NFAT activity and subcellular localization, producing both positive and inhibitory outcomes. The first group includes the MAPK, JNK, or vaccinia-related kinase 2, while negative regulatory kinases include protein kinase A, glycogen synthase kinase 3 (GSK3), casein kinase 1 (CK1), and members of the dual specificity tyrosine-regulated kinase (DYRK) family (reviewed in Shou et al., 2015).

DYRKs are an evolutionarily conserved family of kinases belonging to the CMGC group that participate in signaling pathways that are critical for development and in maintaining cell homeostasis (reviewed in Aranda et al., 2011). There are five members of the mammalian DYRK subfamily (DYRK1A, DYRK1B, DYRK2, DYRK3, and DYRK4) that have distinct expression patterns and, to some extent, different substrate specificity. DYRK1A is the best-studied member of the family due to its link to human pathologies, both when overexpressed as part of the Down syndrome critical region (reviewed in Park and Chung, 2013) or when in haploinsufficiency associated to a complex clinical syndrome (Bronicki et al., 2015). Human DYRK1A and DYRK2 interact with and phosphorylate the regulatory domains of NFAT proteins *in vitro*, priming further CK1 and
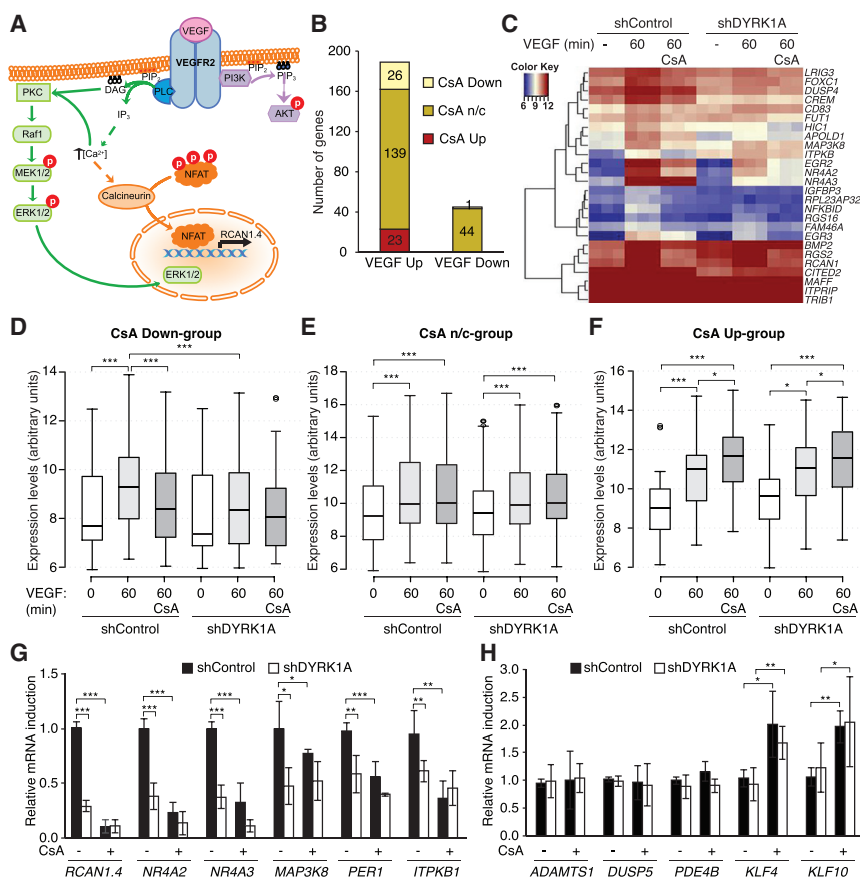
Figure 1. Downregulation of DYRK1A Impairs the Expression of VEGF-Induced NFAT Target Genes

(A) Schematic representation of the main signaling pathways activated by VEGF.

(B) Genes regulated significantly by VEGF were classified as VEGF up- or downregulated genes ($-1.4 > FC > 1.4$, $p < 0.05$) and further subdivided in function of the effect of CsA as CsA-inhibited (CsA Down; $FC < -1.3$, $p < 0.05$), CsA-unchanged (CsA n/c) and CsA-enhanced genes (CsA Up, $FC > 1.3$, $p < 0.05$). See also Figure S2 for further analysis.

(C) Cluster analysis of VEGF-upregulated and CsA-inhibited genes. The color key refers to "normalized intensity" of the microarray data.

(D–F) Boxplots representing the median expression of all the genes in CsA-inhibited (D), Csa-unchanged (E), and CsA-enhanced (F) categories: basal (white), VEGF induced (light gray), and VEGF induced + CsA (dark gray). Center lines show the medians, box limits indicate the 25th and 75th percentiles, whiskers extend 1.5 times the interquartile range from the 25th and 75th percentiles, and outliers are represented by dots (2-way ANOVA with Bonferroni correction for multiple comparisons).

(G and H) Expression of selected genes in the shControl or shDYRK1A-infected HUVECs determined by qRT-PCR in the VEGF up/CsA inhibited group (G) or in the other two groups (H). Data are relative to the induction following VEGF stimulation in shControl cells set arbitrarily as 1 (mean ± SD; n = 3, assayed in triplicate; pairwise comparisons with a two-tailed Mann-Whitney *U* test; see also Figure S2).

GSK3 phosphorylation (Arron et al., 2006; Gwack et al., 2006). DYRK1A and DYRK3 have also been proposed to repress NFAT transcriptional activity in different experimental models of overexpression in the context of pathophysiological NFAT activation such as cardiac hypertrophy, osteoclast differentiation, or pancreatic beta cell replication (Bogacheva et al., 2008; Grebe et al., 2011; Lee et al., 2009; Wang et al., 2015).

Here, we set out to characterize whether DYRKs regulate VEGF-induced Ca²⁺/NFAT signaling in ECs, focusing on DYRK1A. In contrast to what was expected, we found that DYRK1A was required for the correct activation of NFAT upon VEGF stimulation. Downregulation of DYRK1A resulted in less EC proliferation and reduced angiogenesis *in vitro*. In agreement, heterozygous *Dyrk1a* mice responded poorly in *ex vivo* angiogenesis assays and show altered developmental angiogenesis during retinal vasculogenesis. Mechanistically, we show that DYRK1A acts upstream of the increase in intracellular Ca²⁺ induced by VEGF at the level of receptor accumulation.

RESULTS

DYRK1A Is Required for Correct Activation of the Ca²⁺/NFAT Signaling Pathway by VEGF

Phosphorylation of NFAT proteins by DYRK1A and DYRK2 has been shown to be an inactivating event (Arron et al., 2006; Gwack

et al., 2006). Given that NFATs are key downstream effectors of VEGF (Figure 1A), we asked whether DYRK1A might affect transcriptional responses to VEGF-A (hereinafter VEGF) in primary ECs. To this end, RNA microarray analysis was performed using VEGF-stimulated human umbilical vein ECs (HUVECs) infected with a lentivirus expressing a control small hairpin RNA (shRNA) or an shRNA targeting DYRK1A (Figures S1A and S1B). The silencing of DYRK1A did not affect the expression of other DYRKs (Figure S1C), ruling out possible compensatory effects. In addition, as a validation of the experimental setup, the microarray results from noninfected HUVECs were compared with those from shControl-infected ones, demonstrating a large overlap in the VEGF upregulated genes (Figure S1D) and indicating that lentiviral infection per se did not drastically affect the ability of VEGF to induce its transcriptional program.

We focused on those genes induced 1 hr after VEGF stimulation because they are more likely to represent primary transcriptional targets. To discriminate the NFAT-dependent group of genes, we also analyzed VEGF-stimulated cells in the presence of the CN/NFAT inhibitor cyclosporin A (CsA) (Figures S1A and S1B). Analysis of the microarray data showed that 188 genes were significantly upregulated by VEGF in control cells, while 45 genes were downregulated by such stimulation (Figure 1B). Indeed, the data were concordant with earlier expression profiling data for HUVECs stimulated with VEGF (Minami et al.,
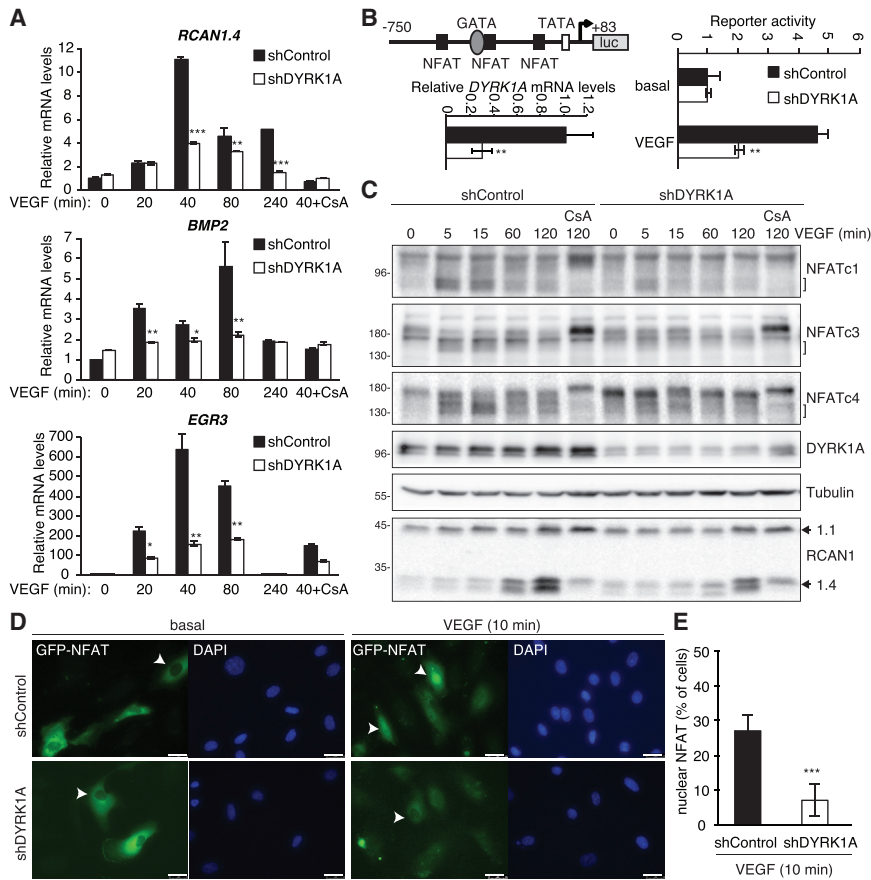
Figure 2. DYRK1A Is Required for NFAT-Dependent Transcriptional Activation

(A) Induction profile of several NFAT-dependent genes analyzed by qRT-PCR in HUVECs stimulated with VEGF; a treatment with CsA is also included. Values of untreated shControl cells were arbitrarily set as 1, and the data correspond to one representative experiment (mean ± SD; DYRK1A knockdown levels are shown in Figure S3A).

(B) Luciferase reporter assays performed in shControl and shDYRK1A cells transiently transfected with a NFAT reporter plasmid (see scheme). The cells were left untreated (basal) or stimulated with VEGF for 6 hr, and the values for the basal condition were set as 1 (mean ± SD of transfection triplicates). DYRK1A knockdown was assessed by qRT-PCR in parallel samples.

(C) Analysis of NFAT proteins in HUVECs stimulated with VEGF. NFAT-hyperphosphorylation was induced by CsA treatment (the brackets indicate the dephosphorylated species). RCAN1 is included as a readout of NFAT activation.

(D and E) Nuclear translocation of a GFP-NFAT fusion protein in shControl and shDYRK1A infected HUVECs (DYRK1A knockdown levels in Figure S3F) induced by VEGF stimulation. Representative images of each condition (D; scale bar, 25 μm) and quantification of cells expressing nuclear GFP-NFAT (E; ~100 cells were counted for each condition; mean ± SD).

2004; Schweighofer et al., 2009). Three groups of genes induced by VEGF were distinguished: genes whose expression did not change significantly in the presence of CsA, genes that were further induced by CsA, and genes whose induction was reduced more than 30% by CsA (Figures 1B–1F; see also Figure S1E). This latter group defines the genes that require NFAT activation for their expression to be induced by VEGF, and it includes already known targets of NFAT such as *RCAN1.4* (Minami et al., 2004; Yang et al., 2000) and other genes that are induced by NFATc1 overexpression or that have NFATc1 occupancy at their proximal promoter regions in HUVECs (Suehiro et al., 2014). When we compared the behavior of these three groups of genes in control cells and DYRK1A-silenced cells, significant changes in VEGF-dependent induction were only observed for the group of genes inhibited by CsA, the activation of which was dampened in the absence of DYRK1A (Figures 1D–1F). qRT-PCR analysis validated the microarray data (Figures 1G and 1H; see also Figure S2) and confirmed that only the genes inhibited by CsA displayed a lower induction in response to VEGF when DYRK1A was silenced.

DYRK1A Depletion Dampens VEGF-Induced NFAT-Dependent Transcriptional Responses

We reasoned that the weaker induction of NFAT targets in DYRK1A silenced cells could be due to a delayed response rather than to reduced transcription. The temporal pattern of

induction was very similar in shDYRK1A cells compared to control cells, but the mRNA levels were reduced at each time point analyzed (Figure 2A; see also Figures S3B and S3C for a parallel assessment of *RCAN1* mRNA and protein), ruling out a delay in transcriptional activation. We next assessed NFAT transcriptional activity more directly by analyzing the activity of a luciferase reporter under the control of the *RCAN1.4* internal promoter, which is known to depend on NFAT activity (Minami et al., 2004). Whereas reporter activity was induced by VEGF in control cells, little activation was observed in cells silenced for DYRK1A (Figure 2B for shRNA treatment and Figure S3D for siRNA), further confirming that the depletion of endogenous DYRK1A impairs VEGF-dependent NFAT activation.

NFAT activation by VEGF requires the dephosphorylation of the NFAT proteins, which can be traced by the appearance of faster-migrating electrophoretic bands sensitive to CN inhibition (CsA treatment) (Figure 2C). An effect of DYRK1A phosphorylation on NFATc1 stability has been reported (Liu et al., 2017), but DYRK1A depletion did not affect NFAT protein accumulation in this cellular context (Figure S3E). However, a reduction was detected in the NFAT protein isoforms with increased electrophoretic mobility, which likely corresponds to the hypophosphorylated forms (Figure 2C). The result is quite surprising given that DYRK1A has been shown to directly phosphorylate NFATs (Arron et al., 2006; Gwack et al., 2006), and hence, an increase in the hypophosphorylated forms when DYRK1A is reduced would be expected. Changes in NFATs phosphorylation are directly responsible of their nucleocytoplasmic transport, with
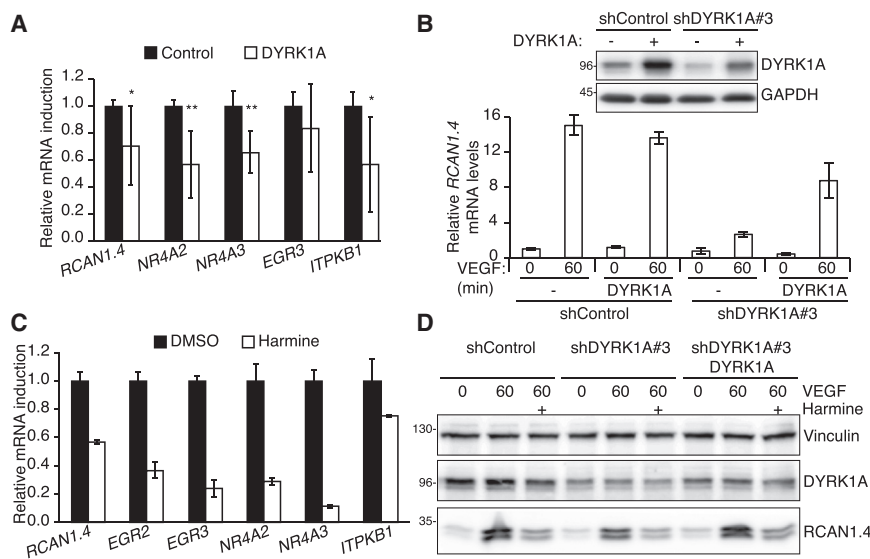
Figure 3. DYRK1A Kinase Activity Is Necessary for NFAT Signaling

(A) Expression of selected genes determined by qRT-PCR in control cells and in cells over-expressing DYRK1A. The induction in control cells after VEGF stimulation was set as 1 (mean ± SD; n = 3 independent experiments; see also Figures S4A and S4B).

(B) *RCAN1.4* mRNA expression upon VEGF stimulation in cells expressing a control shRNA, a shRNA against the 3′ UTR of *DYRK1A* (#3), or in cells co-expressing the shRNAs indicated and a shRNA-resistant DYRK1A (mean ± SD of PCR triplicates in a representative experiment). The changes in DYRK1A were analyzed in western blots (top).

(C) VEGF-dependent induction of NFAT target genes in HUVECs treated for 6 hr with vehicle (DMSO) or harmine (the level of induction in HUVECs stimulated with VEGF in the presence of DMSO was set as 1; mean ± SD of PCR triplicates in a representative experiment; see also Figures S4G and S4H).

(D) Western blot analysis of HUVECs infected with the indicated lentiviruses and stimulated with VEGF in the presence of the vehicle alone or harmine.

dephosphorylated NFATs entering the nucleus upon signaling as illustrated by the nuclear accumulation of a GFP-NFAT fusion protein upon VEGF stimulation (Figure 2D). However, GFP-NFAT nuclear localization was impaired in DYRK1A-silenced cells (Figures 2D and 2E), a result that agrees with the increase in NFAT phosphorylation detected in the immunoblots. Together, these results define an unexpected yet critical role for DYRK1A in the VEGF-induced dephosphorylation of NFAT and its subsequent transcriptional activation.

The Effect of DYRK1A on VEGF Responses Depends on Its Catalytic Activity

DYRK1A overexpression appears to inhibit NFAT activation in different physiological contexts (Arron et al., 2006; Grebe et al., 2011; Gwack et al., 2006; Lee et al., 2009). We assessed this effect in our experimental system. In this case, the effect on the activation of NFAT targets was highly variable from experiment to experiment (Figure 3A); only high levels of DYRK1A dampened VEGF-dependent activation of NFAT targets (Figure S4A), while lower levels did alter neither NFAT phosphorylation nor NFAT target expression (Figures S4A and S4B). In addition, unlike endogenous DYRK1A, which was detected mostly in the cytosol of HUVECs, exogenously expressed DYRK1A accumulated almost exclusively in the nucleus (Figure S4C). It is therefore possible that high levels of exogenously expressed nuclear DYRK1A would drive the phosphorylation of endogenous NFAT and subsequent transcriptional inhibition.

DYRK1A re-expression restored the induction levels of the NFAT target *RCAN1.4* (Figure 3B), and other NFAT targets were partially rescued (Figure S4D). These results argue against off-target effects and clearly establish a dependence on DYRK1A expression. DYRK1A is catalytically active in HUVECs upon VEGF stimulation (Figures S4E and S4F), and thus, we wondered whether the kinase activity is required for DYRK1A-

mediated effects. Unfortunately, we could not get detectable expression of a DYRK1A kinase inactive mutant in HUVECs to evaluate kinase-dependency. As an alternative, prior to VEGF stimulation we exposed HUVECs to harmine, a known inhibitor of DYRK1A kinase activity (Bain et al., 2007; Laguna et al., 2008). Harmine treatment mimicked the effect of DYRK1A down-regulation, as the VEGF-dependent induction of NFAT targets was dampened in harmine-treated cells (Figure 3C), an effect that was enhanced as the pretreatment time increased (Figures S4G and S4H). Moreover, the rescue achieved by DYRK1A re-expression did not occur in the presence of harmine (Figure 3D), confirming that NFAT's ability to induce *RCAN1.4* expression is dependent on DYRK1A kinase activity. Notably, harmine possesses anti-angiogenic activity, as it impedes HUVEC proliferation and tube formation (Dai et al., 2012; Hamsa and Kuttan, 2010), which our results suggest could be due, at least in part, to DYRK1A inhibition. Thus, our data suggest that the kinase activity of DYRK1A is required to modulate VEGF/Ca^{2+}/NFAT signaling in HUVECs.

DYRK1A Modulates a Signaling Step in VEGF Stimulation Upstream of the Release of Ca^{2+} from Intracellular Stores

In ECs, several pro-angiogenic genes, including *RCAN1.4*, are also induced by interleukin-1β (IL-1β) signaling (Schweighofer et al., 2009). Based on our results, the induction of *RCAN1.4* by IL-1β appears to be independent of NFAT activation, as it is not affected by CsA (Figures S5A–S5C). In addition, no effect was observed on the ability of IL-1β to induce *RCAN1.4* in DYRK1A-silenced cells, nor were other common targets of IL-1β and VEGF signaling affected (Figures S5B and S5D). Altogether, these data suggest that the signaling impairment in the activation of pro-angiogenic genes due to DYRK1A downregulation in HUVECs is restricted to the Ca^{2+}/NFAT pathway.
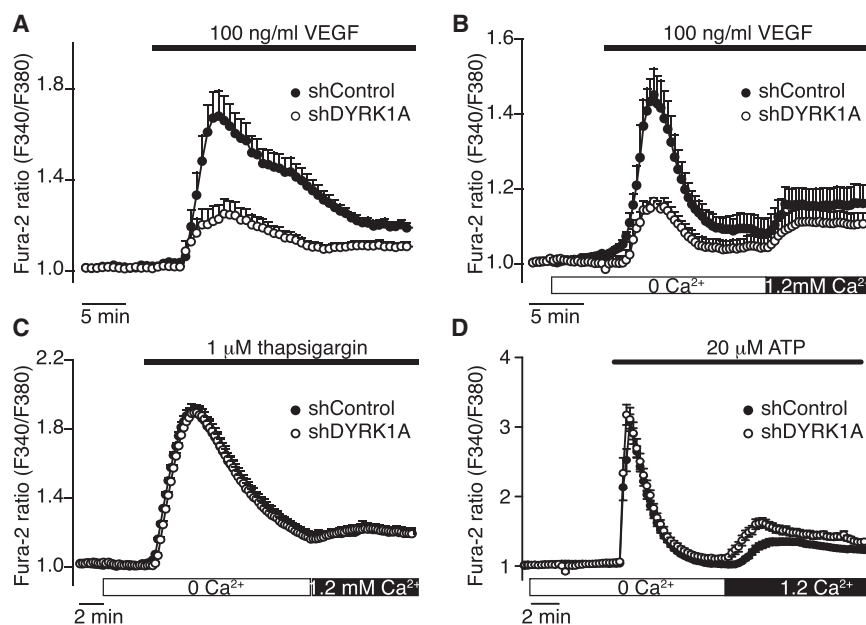
Figure 4. DYRK1A Depletion Results in Impaired Ca^{2+} Mobilization upon VEGF Stimulation

HUVECs infected with shControl or shDYRK1A lentiviruses were growth factor deprived for 6 hr, and intracellular Ca^{2+} mobilization was assayed *in vivo*.

(A) Cells were treated with VEGF in isotonic solution + 1.2 mM Ca^{2+} (mean ± SEM, shControl, n = 45; shDYRK1A, n = 54; p < 0.0001).

(B) Cells were treated with VEGF in a Ca^{2+}-free isotonic solution (0 Ca^{2+}) and then switched to isotonic solution + Ca^{2+} (mean ± SEM, shControl, n = 113; shDRYK1A, n = 112; p < 0.0001).

(C) Cells were treated with TG in a Ca^{2+}-free isotonic solution (0 Ca^{2+}) and then switched to isotonic solution + Ca^{2+} (mean ± SEM, shControl, n = 39; shDYRK1A, n = 41; p > 0.5).

(D) Cells were treated with ATP in a Ca^{2+}-free isotonic solution (0 Ca^{2+}) and then switched to isotonic solution + Ca^{2+} (mean ± SEM, shControl, n = 79; shDYRK1A, n = 65; p > 0.5).

Next, we asked at which level of the VEGF/Ca^{2+}/NFAT pathway DYRK1A is acting. Based on the changes in NFAT phosphorylation, we wondered whether DYRK1A was placed upstream or at the level of CN activation. To evaluate this possibility, we interrogated the pathway when pharmacologically activated: the combination of ionomycin (Io), which allows the passage of Ca^{2+} across membranes, and the protein kinase C agonist phorbol 12-myristate 13-acetate (PMA) induces potent NFAT signaling (Figure S5E). Indeed, HUVECs respond by augmenting *RCAN1.4* transcription, and notably, DYRK1A downregulation did not affect this induction (Figures S5G and S5H). Importantly, the fact that the effects of DYRK1A downregulation on NFAT signaling are overridden when Ca^{2+} freely enters the cell suggests that DYRK1A must act upstream of cytosolic Ca^{2+} release.

To test this hypothesis, we analyzed how depletion of DYRK1A affected intracellular Ca^{2+} mobilization, and we found a strong reduction in cytosolic Ca^{2+} signals in response to VEGF in shDYRK1A-infected cells compared to control cells (Figure 4A). The different components of cytosolic Ca^{2+} signals recorded in response to VEGF were also evaluated with a Ca^{2+} add-back protocol (Figure 4B). While the first peak, corresponding to Ca^{2+} release from intracellular stores (mainly the ER), was clearly reduced in DYRK1A-silenced HUVECs, the entry component following Ca^{2+} addition was unaltered (Figure 4B). To distinguish whether DYRK1A participates in controlling Ca^{2+} accumulation in the ER or VEGF-mediated Ca^{2+} release from the ER, we used the sarco/ER Ca^{2+}-ATPase pump inhibitor thapsigargin (TG). The ability of TG to empty the intracellular stores and the subsequent activation of store-operated Ca^{2+} entry were not different in shControl and shDYRK1A-expressing cells (Figure 4C); in addition, no defects were observed when Ca^{2+} entry was induced with a Ca^{2+} mobilizer as ATP or with ionophore treatment (Figures 4D and S5F). Together, these results indicate

that the lack of DYRK1A prevents Ca^{2+} release from the ER interfering at an upstream signaling step.

DYRK1A-Dependent Modulation of Ca^{2+}/NFAT Signaling Is Mediated at the Level of VEGFR2 Stability

The release of Ca^{2+} from the ER is triggered by the ligand-bound receptor signaling events that lead to the activation of PLCγ. We have previously reported that DYRK1A controls the availability of RTK (EGF receptor) by regulating its half-life (Ferron et al., 2010). Therefore, in a search for the molecular mechanism explaining how DYRK1A might regulate Ca^{2+}/NFAT signaling, we tested whether VEGF receptor (VEGFR2) accumulation was affected by DYRK1A downregulation. As other RTKs, VEGFR2 undergoes endocytosis and subsequent targeting for either recycling or degradation upon ligand binding (reviewed in Simons et al., 2016). Our results showed that VEGFR2 accumulation in response to VEGF was reduced in cells depleted of DYRK1A (Figures 5A and 5B). Concomitant with this reduction, the phosphorylation levels of several of the tyrosine residues involved in VEGFR2-dependent signaling cascades were also reduced (Figures 5A and 5B; see also Figures S6A and S6B). The decrease paralleled VEGFR2 amounts, since the ratio pY1175/total was not significantly different (Figure 5D). In particular, phosphorylated Y1175 in VEGFR2 is the docking site for PLCγ1, and it is crucial to initiate PLCγ1/Ca^{2+} signaling. Accordingly, the reduction in VEGFR2-pY1175 resulted in decreased PLCγ1 activation as measured by reduced Y783 phosphorylation (Figure 5D). Likewise, the activation of downstream signaling pathways was also negatively affected by silencing DYRK1A (Figure 5D).

Notably, no changes in VEGFR2 mRNA were detected in DYRK1A-silenced cells (Figure 5C), indicating that the effect on VEGFR2 accumulation was post-transcriptional. Indeed, degradation of VEGFR2 in cells treated with the protein synthesis inhibitor cycloheximide was enhanced in DYRK1A knockdown
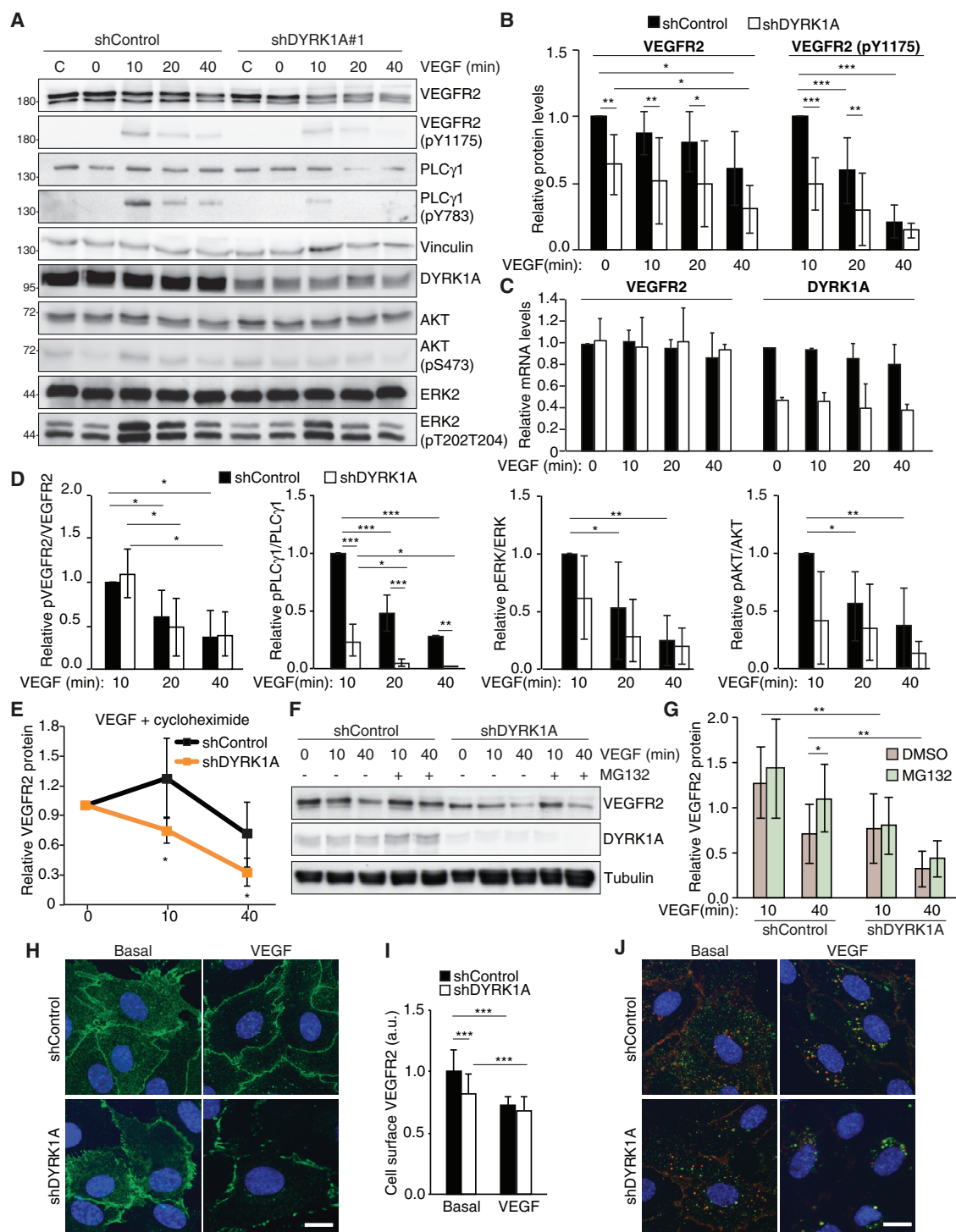
Figure 5. DYRK1A's Effect on Ca2+/NFAT Signaling Is Exerted at the Level of VEGFR2 Accumulation

(A and B) Immunoblot analysis to track the activation of VEGFR2 and downstream effectors. A representative image (A; C refers to normal growing conditions) and the relative quantification of the signals for VEGFR2 and VEGFR2 phosphorylated at Y1175 (B) with respect to the values in shControl cells at t = 0 (total) or t = 10 min (for pY1175) set arbitrarily as 1 (mean ± SD; n = 10; see also Figures S6A and S6B).

(C) *VEGFR2* and *DYRK1A* mRNA levels in HUVECs treated with VEGF. The values in shControl cells at t = 0 were set up as 1 (mean ± SD; n = 2; see also Figure S6C for quantification of cells growing in normal conditions).

(D) Activation of the effectors indicated represented as the ratio of the signals for the phospho-antibodies to the pan-antibodies; the values in shControl cells at t = 10 min were set arbitrarily as 1 (mean ± SD; pVEGFR2/VEGFR2, n = 10; pPLCγ1/PLCγ1, n = 4; pERK/ERK, n = 4; pAKT/AKT, n = 3; 2-way ANOVA with

(legend continued on next page)

cells (Figure 5E), suggesting a higher turnover rate in the absence of DYRK1A. This conclusion is further supported by the fact that the reduced accumulation of VEGFR2 upon VEGF treatment is rescued in the presence of the proteasome inhibitor MG132 and, partially, in cells depleted of DYRK1A (Figures 5F and 5G). Cell-surface levels of VEGFR2 were also reduced in shDYRK1A knockdown cells (Figures 5H and 5I), which could be a reflection of the reduction in total VEGFR2. However, VEGF treatment induced depletion of cell-surface VEGFR2 similarly in both conditions (Figures 5H and 5I), indicating that receptor internalization is active in the absence of DYRK1A. To provide further support, we used an "antibody feeding" assay (Gampel et al., 2006). VEGFR2 molecules exposed in the plasma membrane were labeled with a VEGFR2 extracellular-domain-specific antibody; the signals detected in cells fixed directly after this labeling period correspond to the retention of VEGFR2 at the cell surface (in green in Figure 5J), while the signals detected in cells fixed and permeabilized correspond to internalized VEGFR2 in unstimulated conditions (in red in Figure 5J) and located in the endosomal compartment as previously described (Gampel et al., 2006). Antibody-labeled cells were chased *in vivo* for 40 min with VEGF, which induced an increase in VEGFR2 internalized in control cells consistent with ligand-induced receptor internalization (Figures 5J and S6E). In DYRK1A-silenced cells, although VEGFR2 was internalized in both unstimulated cells and upon VEGF treatment, the increase in the amount of VEGFR internalized was not observed (Figure 5J; see also Figure S6E for quantifications), an effect compatible with increased degradation of the internalized receptor.

We conclude that the reduction in VEGFR2 amounts when DYRK1A is silenced could lead to a reduction in PLCγ1 activation, which in turn would be responsible of the defects observed in intracellular Ca^{2+} mobilization.

DYRK1A Is a Critical Modulator of Angiogenesis

Adequate activation of the Ca^{2+}/NFAT pathway in response to VEGF is required for many steps in the angiogenic process. To test the importance of DYRK1A in this context, we first evaluated the proliferative response of ECs upon DYRK1A downregulation. The increase in cell number provoked by VEGF in shControl samples was not evident in shDYRK1A cells (Figure 6A). In addition, we analyzed HUVEC behavior in Matrigel assays to follow their ability to organize themselves in networks, a model where the

CN/NFAT pathway is known to play a critical role (Rafiee et al., 2004). In agreement with the reduced NFAT response, DYRK1A-depleted cells were virtually unable to organize into cord-like structures *in vitro*, and the effect was largely rescued upon the re-establishment of DYRK1A expression (Figure 6B).

Next, we wanted to assess the impact of DYRK1A activity on angiogenesis in a more physiological manner. Since *Dyrk1a* loss of function is embryonic lethal in mice (Fotaki et al., 2002), we use heterozygous mice, keeping in mind that *DYRK1A* haploinsufficiency is pathological in humans. First, we analyzed how mouse lung ECs (mLECs) obtained from *Dyrk1a*^{+/−} mice responded to VEGF treatment regarding NFAT-response and found that heterozygous cells were unable to induce *Rcan1.4* expression (Figure S7A); in agreement with the data obtained in HUVECs, VEGFR2 protein levels were reduced in the *Dyrk1a*^{+/−} mLEC cultures (Figure S7B). Next, we performed an *ex vivo* aortic ring angiogenesis assay after checking to confirm that DYRK1A is expressed in aortic tissue and reduced in *Dyrk1a*^{+/−} mice (Figure 7A) and that it is detected in aortic ECs (Figure S7C). In accordance with the DYRK1A depletion *in vitro* assays, vessel sprouting was markedly reduced in *Dyrk1a*^{+/−} aortic rings compared to wild-type (Figure 7B; see also Figure S7D), supporting the need for DYRK1A for a full angiogenic response in this model of neoangiogenesis.

The role of DYRK1A was also examined in postnatal retinal angiogenesis, a process that is driven primarily by VEGF. At postnatal day 6 (P6), when the growing vasculature has not yet reached the periphery of the retina, *Dyrk1a* heterozygous retinas showed a reduction in the expansion of the vasculature (Figures 7C and 7D). Interestingly, the number of main vessels was significantly reduced in *Dyrk1a*^{+/−} mice at P6 compared with wild-type littermates (Figures 7E and S7E), with no major differences in NG2 staining. No differences were observed in the number of sprouts or in the branching points when the two genotypes were compared (Figures 7F and 7G). By P11, vascular sprouts have already invaded deep retina layers in wild-type retinas, and the vascular plexus has undergone significant remodeling (Figures 7H and 7I). In contrast, *Dyrk1a*^{+/−} retinas showed an immature vascular plexus; the sprouting front had not even reached the periphery of the retina (Figure 7H), and the intermediate vascular plexus not even formed (Figure 7I).

The *Dyrk1a* loss-of-function mouse model is not endothelial specific, and it is known that other cell types, such as retinal

Bonferroni correction for multiple comparisons; the comparison between shControl and shDYRK1A for ERK and AKT is statistically significant in pairwise comparisons with non-parametric tests).

(E) Quantification of VEGFR2 in cells incubated with cycloheximide for 30 min and stimulated with VEGF for the indicated times. The protein level in basal conditions (t = 0) is set as 1 (mean ± SD; n = 5).

(F and G) HUVECs infected with shControl and shDYRK1A lentiviruses were incubated in basal medium for 6 hr in the presence of the protein synthesis inhibitor cycloheximide for 30 min before VEGF treatment. When indicated, the cells were also incubated in the presence of the proteasome inhibitor MG132. The blots correspond to a representative experiment (F), and the graph (G) is the quantification of 4 independent experiments (mean ± SD).

(H) Localization of VEGFR2 at the cell surface as determined by immunofluorescence with an antibody against the extracellular domain of VEGFR2 (green) in untreated cells (basal) and after 40 min of VEGF treatment. Nuclei are shown in blue (scale bar, 100 μm).

(I) For quantification of cell-surface VEGFR2, the values are expressed in arbitrary units (integrated intensity of the area in each cell) and referred to the values in shControl cells in basal conditions (mean ± SD; n = 100–150 cells per each condition from 2 independent experiments; one-way ANOVA). See also Figure S6D for quantification in cells growing in normal conditions.

(J) Endocytosis of VEGFR2 visualized by an antibody-feeding assay in serum-starved cells or in cells stimulated for 40 min with VEGF. Localization of VEGFR2 at the cell surface is determined in cells fixed (green), whereas detection of internalized VEGFR2 was done in cells fixed and permeabilized (red). Nuclei are shown in blue (scale bar, 100 μm). See Figure S6E for quantification.
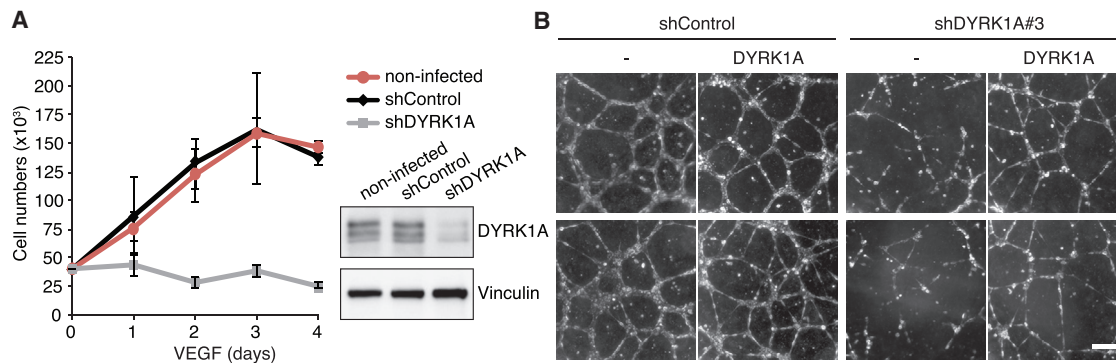
Figure 6. DYRK1A Is Required for the Angiogenic Response of ECs
(A) Cell growth curves of HUVECs not infected (red), infected with shControl (black), or shDYRK1A (gray) plated in response to VEGF (plating day is 0; mean ± SD; n = 2 independent experiments performed in triplicate). The level of DYRK1A depletion was assessed by western blot (see also Figure S6F for growth in the absence of VEGF).
(B) shControl and shDYRK1A-infected HUVECs were re-infected with a control lentivirus or a lentivirus expressing DYRK1A and analyzed in 2D Matrigel assays. Scale bar, 100 μm. (DYRK1A levels are shown in Figure S6G; see also Figures S6H–S6J for results with independent shRNAs to DYRK1A).

astrocytes, play an important role in the development of the mammalian retinal vasculature (Watanabe and Raff, 1988). DYRK1A is expressed in all neural cell types in the developing retina, including astrocytes (Laguna et al., 2008); therefore, it is possible that the observed phenotype is the result of defects not only in ECs but also in astrocytes. The analysis of the astrocytic network at P5 using PDGFRα as marker showed that whereas the vascular expansion was already affected at this postnatal age (as assessed by measuring IB4 staining), no differences were observed in the expansion of the astrocyte front when $Dyrk1a^{+/-}$ retinas were compared to wild-type retinas (Figures S7F and S7G). Thus, although we cannot rule out that a combination of endothelial and nonendothelial effects could contribute to the phenotypic differences between $Dyrk1a^{+/+}$ and $Dyrk1a^{+/-}$ mice, we think that altogether, the data support a role for DYRK1A in physiological angiogenesis.

DISCUSSION

In the present study, we found that downregulation of DYRK1A kinase and inhibition of its activity severely affect VEGF-dependent signaling in ECs and their homeostasis. The *in vitro* effects have a relevant correlation *in vivo*, since we show a strong impact in physiological angiogenesis in a $Dyrk1a$ haploinsufficiency model. Furthermore, we reveal an unexpected role for DYRK1A as a positive regulator of VEGF-dependent NFAT activation in ECs. Indeed, our results indicate that endogenous DYRK1A is required for the appropriate mobilization of Ca^{2+} from intracellular stores in response to VEGF, given that DYRK1A depletion reduces the Ca^{2+} spike resulting from ER Ca^{2+} release without affecting extracellular Ca^{2+} influx; our data are compatible with this effect being the result of the DYRK1A-dependent control of VEGFR2 accumulation and downstream PLCγ1 activation.

Transcriptional profiling of VEGF-stimulated HUVECs showed that only a particular subset of the genes induced (those repressed by CsA) was sensitive to DYRK1A downregulation. The fact that NFAT proteins showed reduced dephosphorylation and nuclear translocation following VEGF treatment in DYRK1A-

depleted cells has allowed us to establish a molecular link between the smaller increase in intracellular Ca^{2+} and the reduced NFAT-dependent transcriptional activation. This positive role for DYRK1A in NFAT signaling is quite unexpected given its accepted role as an inhibitory NFAT kinase (Arron et al., 2006; Gwack et al., 2006; Kuhn et al., 2009; Lee et al., 2009; Stefos et al., 2013). Several explanations may account for the apparent discrepancy. First, most functional associations reported previously are based on DYRK1A overexpression. Our analysis in different cellular systems indicates that ectopically expressed DYRK1A accumulates in the nucleus (Alvarez et al., 2003), while it is mostly cytosolic in endogenous conditions, as we show here for HUVECs. It is therefore possible that strong overexpression might favor nuclear interactions that do not necessarily take place in physiological conditions. In fact, we only observe the inhibition of VEGF/NFAT targets when DYRK1A is strongly overexpressed, possibly indicating that such inhibition relies on increased NFAT phosphorylation in the nucleus as shown by others (Arron et al., 2006; Gwack et al., 2006). Second, the conditions used for NFAT activation, such as constitutively active CN or TG, override the physiological activation of the pathway and render it independent of the step defined here. Third, the effect of DYRK1A on NFAT activation might depend on the cellular context and/or stimulus. Hence, the functional interaction of DYRK1A with distinct sets of positive and/or negative regulators within the signaling cascades could have distinct biological consequences. This might explain why the DYRK inhibitor harmine potentiates RANKL-induced NFAT activation in RAW264.7 cells (Egusa et al., 2011), whereas we show here that it inhibits NFAT activation by VEGF in HUVECs. Noteworthy, DYRK1A is a highly dosage-sensitive kinase, and although some of the phenotypes associated with DYRK1A deregulation are linear in terms of dosage (Laguna et al., 2008), the same phenotypic output has also been observed with both its overexpression and downregulation in certain paradigms (Chen et al., 2013).

From the mechanistic point of view, our results suggest that DYRK1A's effect on VEGF signaling is exerted at the level of VEGFR2 accumulation, which affects the levels of the receptor
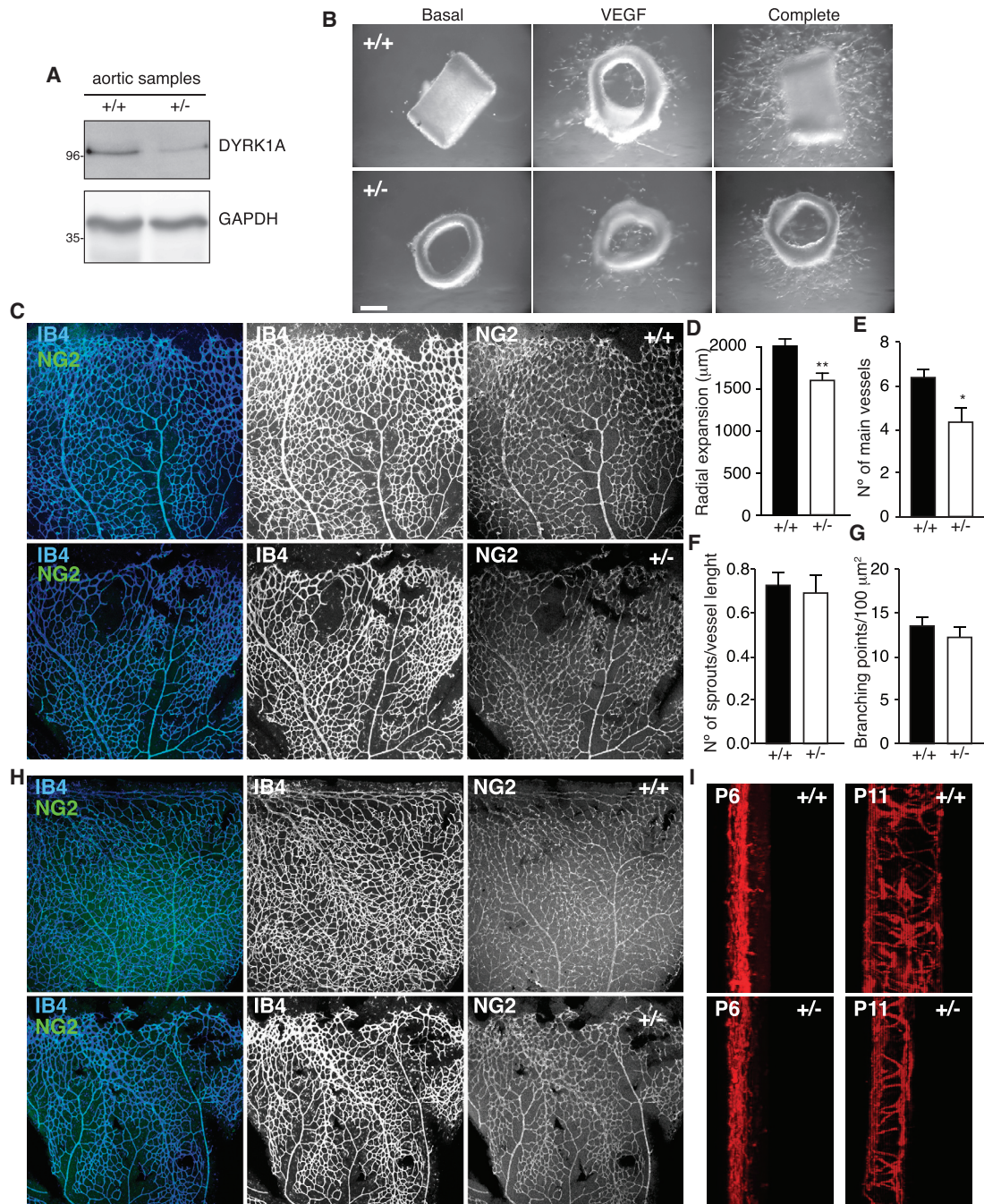
Figure 7. *Dyrk1a* Heterozygous Mice Show Defects in Angiogenic Responses

(A) DYRK1A expression in aortic extracts from wild-type and $Dyrk1a^{+/-}$ mice analyzed by western blot.

(B) Aortic ring assays from $Dyrk1a^{+/-}$ female mice or their wild-type littermates performed in 2% FCS without (basal) or with VEGF, or in complete growth medium (Complete). A representative picture of each condition is shown (scale bar, 0.2 mm; see also Figure S7D).

(C) Visualization of the vasculature by isolectin B4 immunofluorescence (EC membrane) and NG2 staining (pericytes) in retinas from wild-type and $Dyrk1a^{+/-}$ mice at P6.

(D–G) Quantification of several features of the retinal vasculature at P6 in $Dyrk1a^{+/+}$ and $Dyrk1a^{+/-}$ animals; radial expansion (D; n = 5 for each genotype), number of main vessels (E; +/+, n = 5; +/−, n = 4; see also Figure S7E for representative images), number of sprouts (F; n = 5 for each genotype), and branch points (G; n = 5 for each genotype) (mean ± SEM).

(H) Visualization of the vasculature by IB4 and NG2 staining in retinas from wild-type and $Dyrk1a^{+/-}$ mice at P11.

(I) Transversal view of CD31 stained retinas at P6 and P11 obtained by 3D reconstruction of z-projection of confocal images covering the whole thickness of retinal vasculature, showing the formation of the deep an intermediate plexus in wild-type and $Dyrk1a^{+/-}$ mice.

at the cell surface. This results in a reduction in PLCγ1 activation, likely due to the diminished presence of VEGFR2-pY1175 molecules. Reduced PLCγ1 activation would affect Ca^{2+} mobilization, which would ultimately be responsible for the impaired NFAT-transcriptional response. Given that the effect of DYRK1A appears not to be an on/off effect, the kinase could participate in a mechanism regulating the amplitude or the duration of Ca^{2+} signaling and, hence, the activation of specific NFAT targets (Kar and Parekh, 2015; Yissachar et al., 2013). VEGFR2 internalizes efficiently in serum-starved HUVECs independently of ligand and upon VEGF stimulation (Basagiannis and Christoforidis, 2016). In addition, ligand-independent VEGFR2 ubiquitination has been linked to receptor membrane trafficking and proteolysis (Smith et al., 2017). However, it is not clear whether the constitutive VEGFR2 and the ligand-induced internalization/degradation pathways share mechanisms and effectors. We observed reduction of VEGFR2 in both serum-starved HUVECs and upon VEGF treatment; however, we think that the half-life measurements in VEGF-treated cells allow us to safely propose that DYRK1A protects VEGFR2 from the internalization-associated degradation of the receptor that follows ligand binding. Currently, we cannot precisely define at which of the steps that regulate VEGFR2 accumulation DYRK1A is acting: receptor internalization, intracellular trafficking, targeting to the proteasome/lysosome degradation pathway, or recycling to the membrane. However, the protective role of DYRK1A in VEGFR2 homeostasis is quite comparable to that on EGF receptor in adult neural stem cells or glioblastoma (Ferron et al., 2010; Pozo et al., 2013) and could be an indication of a more general role of DYRK1A on the regulation of RTK's stability. Finally, we are aware that given the pleiotropic nature of DYRK1A, our data do not rule out other potential mechanisms, related or not to the regulation of NFAT activity, that contribute to the participation of DYRK1A in angiogenesis.

In summary, our results are consistent with DYRK1A being required for angiogenesis. Further *in vivo* analysis will be necessary to fully elucidate the role of DYRK1A in physiological angiogenesis and whether DYRK1A is important in pathological conditions associated with angiogenesis, such as tumor-associated neovascularization and other angiogenesis-related diseases. Such studies will surely provide valuable information on the potential of using DYRK1A as a target for the therapeutic manipulation of angiogenesis.

EXPERIMENTAL PROCEDURES

Cell Culture and Cell-Based Procedures
HUVECs were obtained from Lonza and maintained in EGM-2 BulletKit complete Medium (Lonza). Cell treatments and extract preparation were done at 80% confluency. For growth curves, cells were plated at 4,000 cells/cm² in triplicate (day 0) and counted every 24 hr for 4 days. Transient DYRK1A downregulation was achieved by small interfering RNA (siRNA) transfection using Lipofectamine 3000. The siRNAs used were a control non-targeting pool (D-001810-10) or a human DYRK1A SMARTpool (L-004805-00) obtained from Dharmacon. Cell treatments were performed in basal EBM-2 medium (Lonza) supplemented with 2% fetal calf serum (FCS) (see Supplemental Experimental Procedures for conditions). See also Supplemental Experimental Procedures for lentivirus stock preparation and infection and conditions for 2D *in vitro* Matrigel assays. Intracellular Ca^{2+} was measured as described previously (Jung et al., 2011). Mouse primary ECs were pre-

pared from lungs of $Dyrk1a^{+/-}$ and wild-type littermates as described previously (Serra et al., 2015).

Animals
We used adult female $Dyrk1a^{+/-}$ mice (Fotaki et al., 2002) and their respective wild-type littermates. The animals were maintained on their original genetic background by repeated backcrossing of $Dyrk1a^{+/-}$ males to C57BL6/Jx129S2/SvHsd F1 females (Harlan Laboratories); animals were genotyped by PCR. All experimental procedures were carried out in accordance with European Union guidelines (Directive 2010/63/EU). The protocols were approved by the Ethics Committee of the CSIC and the IDIBELL.

Microarray Analysis and Quantification of mRNA
RNA samples for microarray analysis (three biological repeats of each sample) were prepared from HUVECs according to the experimental conditions indicated in Figure S1. A complete description of microarray processing and analysis is provided in Supplemental Experimental Procedures. For mRNA quantification, qPCR reactions were performed with SYBR green on cDNA prepared from total RNA and specific oligonucleotides (sequences are provided in Table S1). Each sample was assayed in triplicate, and the threshold cycle (Ct) was calculated using the Relative Quantification of the 2nd Derivative Maximum method with Lightcycler 480 1.2 software (Roche). All results were normalized to *GAPDH* or *ACTB* expression for HUVECs and *Ppia* for mouse samples.

Protein Analysis
A complete description for western blot analysis and *in vitro* kinase assays is provided in Supplemental Experimental Procedures. Antibody sources are listed in Table S2. Immunofluorescence studies were performed as described previously (Aranda et al., 2008; see also Supplemental Experimental Procedures). Information on visualization and quantification of the retinal vasculature is also included.

Statistics
The statistical package included in GraphPad Prism 6 was used. Normality of sample data was evaluated with a D'Agostino and Pearson omnibus test. If samples passed the normality test, a two-tailed unpaired Student's t test was used; if not, significant differences were defined in pairwise comparisons using a two-tailed Mann-Whitney U test. For multiple comparisons, a one-way ANOVA with Bonferroni corrections was used. The data in the graphs represent the mean ± SD of independent experiments. A p value < 0.05 was considered significant (*p < 0.05; **p < 0.001; ***p < 0.0001). All experiments were performed independently at least three times.

Data and Software Accessibility
The accession number for the microarray data reported in this paper is GEO: GSE112172.

SUPPLEMENTAL INFORMATION

Supplemental Information includes Supplemental Experimental Procedures, seven figures, and two tables and can be found with this article online at https://doi.org/10.1016/j.celrep.2018.04.008.

ACKNOWLEDGMENTS

AUTHOR CONTRIBUTIONS

Conceptualization, S.L.; Investigation, E.J.R., J.R., M.J.B., C.D.V., C.J., A.F.F., and J.L.; Writing – Original Draft, E.J.R. and S.L.; Writing – Review & Editing, J.R., C.D.V., and S.L.; Funding Acquisition and Supervision, M.L.A., C.F., M.G., M.A.V., and S.L.

DECLARATION OF INTERESTS

The authors declare no competing interests.

REFERENCES

Alvarez, M., Estivill, X., and de la Luna, S. (2003). DYRK1A accumulates in splicing speckles through a novel targeting signal and induces speckle disassembly. J. Cell Sci. 116, 3099–3107.

Aranda, S., Alvarez, M., Turró, S., Laguna, A., and de la Luna, S. (2008). Sprouty2-mediated inhibition of fibroblast growth factor signaling is modulated by the protein kinase DYRK1A. Mol. Cell. Biol. 28, 5899–5911.

Aranda, S., Laguna, A., and de la Luna, S. (2011). DYRK family of protein kinases: evolutionary relationships, biochemical properties, and functional roles. FASEB J. 25, 449–462.

Arron, J.R., Winslow, M.M., Polleri, A., Chang, C.P., Wu, H., Gao, X., Neilson, J.R., Chen, L., Heit, J.J., Kim, S.K., et al. (2006). NFAT dysregulation by increased dosage of DSCR1 and DYRK1A on chromosome 21. Nature 441, 595–600.

Bain, J., Plater, L., Elliott, M., Shpiro, N., Hastie, C.J., McLauchlan, H., Klevernic, I., Arthur, J.S., Alessi, D.R., and Cohen, P. (2007). The selectivity of protein kinase inhibitors: a further update. Biochem. J. 408, 297–315.

Basagiannis, D., and Christoforidis, S. (2016). Constitutive endocytosis of VEGFR2 protects the receptor against shedding. J. Biol. Chem. 291, 16892–16903.

Bogacheva, O., Bogachev, O., Menon, M., Dev, A., Houde, E., Valoret, E.I., Prosser, H.M., Creasy, C.L., Pickering, S.J., Grau, E., et al. (2008). DYRK3 dual-specificity kinase attenuates erythropoiesis during anemia. J. Biol. Chem. 283, 36665–36675.

Bronicki, L.M., Redin, C., Drunat, S., Piton, A., Lyons, M., Passemard, S., Baumann, C., Faivre, L., Thevenon, J., Rivière, J.B., et al. (2015). Ten new cases further delineate the syndromic intellectual disability phenotype caused by mutations in DYRK1A. Eur. J. Hum. Genet. 23, 1482–1487.

Chen, J.Y., Lin, J.R., Tsai, F.C., and Meyer, T. (2013). Dosage of Dyrk1a shifts cells within a p21-cyclin D1 signaling map to control the decision to enter the cell cycle. Mol. Cell 52, 87–100.

Dai, F., Chen, Y., Song, Y., Huang, L., Zhai, D., Dong, Y., Lai, L., Zhang, T., Li, D., Pang, X., et al. (2012). A natural small molecule harmine inhibits angiogenesis and suppresses tumour growth through activation of p53 in endothelial cells. PLoS ONE 7, e52162.

Egusa, H., Doi, M., Saeki, M., Fukuyasu, S., Akashi, Y., Yokota, Y., Yatani, H., and Kamisaki, Y. (2011). The small molecule harmine regulates NFATc1 and Id2 expression in osteoclast progenitor cells. Bone 49, 264–274.

Ferron, S.R., Pozo, N., Laguna, A., Aranda, S., Porlan, E., Moreno, M., Fillat, C., de la Luna, S., Sánchez, P., Arbonés, M.L., and Fariñas, I. (2010). Regulated segregation of kinase Dyrk1A during asymmetric neural stem cell division is critical for EGFR-mediated biased signaling. Cell Stem Cell 7, 367–379.

Fotaki, V., Dierssen, M., Alcántara, S., Martínez, S., Martí, E., Casas, C., Visa, J., Soriano, E., Estivill, X., and Arbonés, M.L. (2002). Dyrk1A haploinsufficiency affects viability and causes developmental delay and abnormal brain morphology in mice. Mol. Cell. Biol. 22, 6636–6647.

Gampel, A., Moss, L., Jones, M.C., Brunton, V., Norman, J.C., and Mellor, H. (2006). VEGF regulates the mobilization of VEGFR2/KDR from an intracellular endothelial storage compartment. Blood 108, 2624–2631.

Grebe, C., Klingebiel, T.M., Grau, S.P., Toischer, K., Didié, M., Jacobshagen, C., Dullin, C., Hasenfuss, G., and Seidler, T. (2011). Enhanced expression of DYRK1A in cardiomyocytes inhibits acute NFAT activation but does not prevent hypertrophy in vivo. Cardiovasc. Res. 90, 521–528.

Gwack, Y., Sharma, S., Nardone, J., Tanasa, B., Iuga, A., Srikanth, S., Okamura, H., Bolton, D., Feske, S., Hogan, P.G., and Rao, A. (2006). A genome-wide Drosophila RNAi screen identifies DYRK-family kinases as regulators of NFAT. Nature 441, 646–650.

Hamsa, T.P., and Kuttan, G. (2010). Harmine inhibits tumour specific neo-vessel formation by regulating VEGF, MMP, TIMP and pro-inflammatory mediators both in vivo and in vitro. Eur. J. Pharmacol. 649, 64–73.

Herbert, S.P., and Stainier, D.Y. (2011). Molecular control of endothelial cell behaviour during blood vessel morphogenesis. Nat. Rev. Mol. Cell Biol. 12, 551–564.

Jung, C., Gené, G.G., Tomás, M., Plata, C., Selent, J., Pastor, M., Fandos, C., Senti, M., Lucas, G., Elosua, R., and Valverde, M.A. (2011). A gain-of-function SNP in TRPC4 cation channel protects against myocardial infarction. Cardiovasc. Res. 91, 465–471.

Kar, P., and Parekh, A.B. (2015). Distinct spatial Ca2+ signatures selectively activate different NFAT transcription factor isoforms. Mol. Cell 58, 232–243.

Kuhn, C., Frank, D., Will, R., Jaschinski, C., Frauen, R., Katus, H.A., and Frey, N. (2009). DYRK1A is a novel negative regulator of cardiomyocyte hypertrophy. J. Biol. Chem. 284, 17320–17327.

Laguna, A., Aranda, S., Barallobre, M.J., Barhoum, R., Fernández, E., Fotaki, V., Delabar, J.M., de la Luna, S., de la Villa, P., and Arbonés, M.L. (2008). The protein kinase DYRK1A regulates caspase-9-mediated apoptosis during retina development. Dev. Cell 15, 841–853.

Lee, Y., Ha, J., Kim, H.J., Kim, Y.S., Chang, E.J., Song, W.J., and Kim, H.H. (2009). Negative feedback Inhibition of NFATc1 by DYRK1A regulates bone homeostasis. J. Biol. Chem. 284, 33343–33351.

Liu, H., Wang, K., Chen, S., Sun, Q., Zhang, Y., Chen, L., and Sun, X. (2017). NFATc1 phosphorylation by DYRK1A increases its protein stability. PLoS ONE 12, e0172985.

Minami, T., Horiuchi, K., Miura, M., Abid, M.R., Takabe, W., Noguchi, N., Kohro, T., Ge, X., Aburatani, H., Hamakubo, T., et al. (2004). Vascular endothelial growth factor- and thrombin-induced termination factor, Down syndrome critical region-1, attenuates endothelial cell proliferation and angiogenesis. J. Biol. Chem. 279, 50537–50554.

Müller, M.R., and Rao, A. (2010). NFAT, immunity and cancer: a transcription factor comes of age. Nat. Rev. Immunol. 10, 645–656.

Park, J., and Chung, K.C. (2013). New perspectives of Dyrk1A role in neurogenesis and neuropathologic features of Down syndrome. Exp. Neurobiol. 22, 244–248.

Pozo, N., Zahonero, C., Fernández, P., Liñares, J.M., Ayuso, A., Hagiwara, M., Pérez, A., Ricoy, J.R., Hernández-Laín, A., Sepúlveda, J.M., and Sánchez-Gómez, P. (2013). Inhibition of DYRK1A destabilizes EGFR and reduces EGFR-dependent glioblastoma growth. J. Clin. Invest. 123, 2475–2487.

Rafiee, P., Heidemann, J., Ogawa, H., Johnson, N.A., Fisher, P.J., Li, M.S., Otterson, M.F., Johnson, C.P., and Binion, D.G. (2004). Cyclosporin A differentially inhibits multiple steps in VEGF induced angiogenesis in human microvascular endothelial cells through altered intracellular signaling. Cell Commun. Signal. 2, 3.

Schweighofer, B., Testori, J., Sturtzel, C., Sattler, S., Mayer, H., Wagner, O., Bilban, M., and Hofer, E. (2009). The VEGF-induced transcriptional response comprises gene clusters at the crossroad of angiogenesis and inflammation. Thromb. Haemost. *102*, 544–554.

Serra, H., Chivite, I., Angulo-Urarte, A., Soler, A., Sutherland, J.D., Arruabar-rena-Aristorena, A., Ragab, A., Lim, R., Malumbres, M., Fruttiger, M., et al. (2015). PTEN mediates Notch-dependent stalk cell arrest in angiogenesis. Nat. Commun. *6*, 7935.

Shou, J., Jing, J., Xie, J., You, L., Jing, Z., Yao, J., Han, W., and Pan, H. (2015). Nuclear factor of activated T cells in cancer development and treatment. Cancer Lett. *361*, 174–184.

Simons, M., Gordon, E., and Claesson-Welsh, L. (2016). Mechanisms and regulation of endothelial VEGF receptor signalling. Nat. Rev. Mol. Cell Biol. *17*, 611–625.

Smith, G.A., Fearnley, G.W., Abdul-Zani, I., Wheatcroft, S.B., Tomlinson, D.C., Harrison, M.A., and Ponnambalam, S. (2017). Ubiquitination of basal VEGFR2 regulates signal transduction and endothelial function. Biol. Open *6*, 1404–1415.

Soboloff, J., Rothberg, B.S., Madesh, M., and Gill, D.L. (2012). STIM proteins: dynamic calcium signal transducers. Nat. Rev. Mol. Cell Biol. *13*, 549–565.

Stefos, G.C., Soppa, U., Dierssen, M., and Becker, W. (2013). NGF upregu-lates the plasminogen activation inhibitor-1 in neurons via the calcineurin/

NFAT pathway and the Down syndrome-related proteins DYRK1A and RCAN1 attenuate this effect. PLoS ONE *8*, e67470.

Suehiro, J., Kanki, Y., Makihara, C., Schadler, K., Miura, M., Manabe, Y., Abur-atani, H., Kodama, T., and Minami, T. (2014). Genome-wide approaches reveal functional vascular endothelial growth factor (VEGF)-inducible nuclear factor of activated T cells (NFAT) c1 binding to angiogenesis-related genes in the endothelium. J. Biol. Chem. *289*, 29044–29059.

Wang, P., Alvarez-Perez, J.C., Felsenfeld, D.P., Liu, H., Sivendran, S., Bender, A., Kumar, A., Sanchez, R., Scott, D.K., Garcia-Ocaña, A., and Stewart, A.F. (2015). A high-throughput chemical screen reveals that harmine-mediated in-hibition of DYRK1A increases human pancreatic beta cell replication. Nat. Med. *21*, 383–388.

Watanabe, T., and Raff, M.C. (1988). Retinal astrocytes are immigrants from the optic nerve. Nature *332*, 834–837.

Yang, J., Rothermel, B., Vega, R.B., Frey, N., McKinsey, T.A., Olson, E.N., Bas-sel-Duby, R., and Williams, R.S. (2000). Independent signals control expres-sion of the calcineurin inhibitory proteins MCIP1 and MCIP2 in striated muscles. Circ. Res. *87*, E61–E68.

Yissachar, N., Sharar Fischler, T., Cohen, A.A., Reich-Zeliger, S., Russ, D., Shi-frut, E., Porat, Z., and Friedman, N. (2013). Dynamic response diversity of NFAT isoforms in individual living cells. Mol. Cell *49*, 322–330.